doi:10.26443/seismica.v2i2.1086

Red-light thresholds for induced seismicity in the UK

Ryan Schultz [*1], **Brian Baptie** [2], **Benjamin Edwards** [3], **Stefan Wiemer** [1]

[1]Department of Earth Sciences, Swiss Seismological Service, ETH Zürich, Zürich, Switzerland, [2]British Geological Survey, Edinburgh, United Kingdom, [3]School of Environmental Sciences, University of Liverpool, Liverpool, United Kingdom

Author contributions: *Conceptualization*: R. Schultz. *Data Curation*: R. Schultz, B. Baptie, B. Edwards. *Formal Analysis*: R. Schultz. *Funding Acquisition*: S. Wiemer. *Investigation*: R. Schultz. *Methodology*: R. Schultz, B. Edwards. *Project Administration*: R. Schultz. *Resources*: R. Schultz, B. Baptie. *Software*: R. Schultz, B. Edwards. *Supervision*: B. Baptie, S. Wiemer. *Validation*: R. Schultz. *Visualization*: R. Schultz. *Writing – original draft*: R. Schultz. *Writing – review & editing*: R. Schultz, B. Baptie, B. Edwards, S. Wiemer.

Abstract Induced earthquakes pose a serious hurdle to subsurface energy development. Concerns about induced seismicity led to terminal public opposition of hydraulic fracturing in the UK. Traffic light protocols (TLPs) are typically used to manage these risks, with the red-light designed as the last-possible stopping-point before exceeding a risk tolerance. We simulate trailing earthquake scenarios for the UK, focusing on three risk metrics: nuisance, damage, and local personal risk (LPR) – the likelihood of building collapse fatality for an individual. The severity of these risks can spatially vary (by orders-of-magnitude), depending on exposure. Estimated risks from the Preston New Road earthquakes are used to calibrate our UK earthquake risk tolerances, which we find to be comparable to Albertan (Canadian) tolerances. We find that nuisance and damage concerns supersede those from fatality and that the safest regions for Bowland Shale development would be along the east coast. A retrospective comparison of our TLP result with the Preston New Road case highlights the importance of red-light thresholds that adapt to new information. Overall, our findings provide recommendations for red-light thresholds (M_L 1.2-2.5) and proactive management of induced seismicity – regardless of anthropogenic source.

Production Editor: Gareth Funning
Handling Editor: Stephen Hicks
Copy & Layout Editor: Théa Ragon

Signed reviewer(s): James Verdon

Received: July 12, 2023
Accepted: October 4, 2023
Published: October 16, 2023

Non-technical summary Consideration of energy security briefly led the UK to reconsider its moratorium on shale gas hydraulic fracturing (HF) in 2022. HF has the potential to induce earthquakes, which originally led to the UK's moratorium, and could potentially threaten the future of other clean energy technologies. Based on these concerns, we model the potential for induced earthquake risks (nuisance impacts, building damage, and chance of fatality). We also use the experience from the previous earthquakes to calibrate the UK tolerance to these risks. These risk metrics/tolerances are combined to determine when an HF operation should stop: *i.e.*, the red-light threshold, reported as an earthquake magnitude. Our results suggest that the red-light threshold should change with location (M_L 1.2-2.5), primarily due to exposure from ground shaking varying with the distribution of population density. Nuisance and damage are likely the most important risk metrics to consider because they result in the lowest red-light magnitudes. We discuss how our approach could be used to choose HF locations and adapt to real-time information. Overall, our results provide a blueprint for the regulation of future induced earthquakes – including green technologies like geothermal or carbon/hydrogen storage.

1 Introduction

Earthquakes can be induced by anthropogenic activities such as mining, wastewater disposal, and geothermal systems (Foulger et al., 2018). Hydraulic fracturing (HF), a petroleum extraction technique that stimulates fractures by injecting fluids into the subsurface under high pressure (Bickle et al., 2012), has also been documented to cause earthquakes (Atkinson et al., 2020; Schultz et al., 2022b). Yet, most HF operations do not cause noteworthy (*e.g.*, felt) earthquakes (Atkinson et al., 2016; Verdon and Rodríguez-Pradilla, 2023) and only susceptible regions appear to preferentially host larger induced events (Schultz et al., 2018; Pawley et al., 2018). Some cases of HF induced seismicity have hosted moderate magnitude events (M3+) that have been felt, or even damaging. For instance, the current largest documented case to date was the December 2018 M_L 5.7 event in the Sichuan Basin of China (Lei et al., 2019), which caused ~$7M USD in direct economic losses alongside human loss and injuries. Concerns around the risks of induced earthquakes have stymied resource development, in some cases even resulting in moratoriums or resource abandonment.

The UK has a controversial history of HF (Williams et al., 2017) and related induced earthquakes, despite prior tectonic (and coal mining induced) seismicity (Figure 1). The most prospective shale gas target in the UK is the Mississippian aged Bowland Shale (Smith et al., 2010; Andrews, 2013). The first shale gas exploration licenses were awarded in 2008, with the first well (Preese Hall 1, PH-1) targeting the Bowland Shale near Blackpool, Lancashire (Baptie et al., 2022). Stage stimu-

*Corresponding author: Ryan.Schultz@sed.ethz.ch

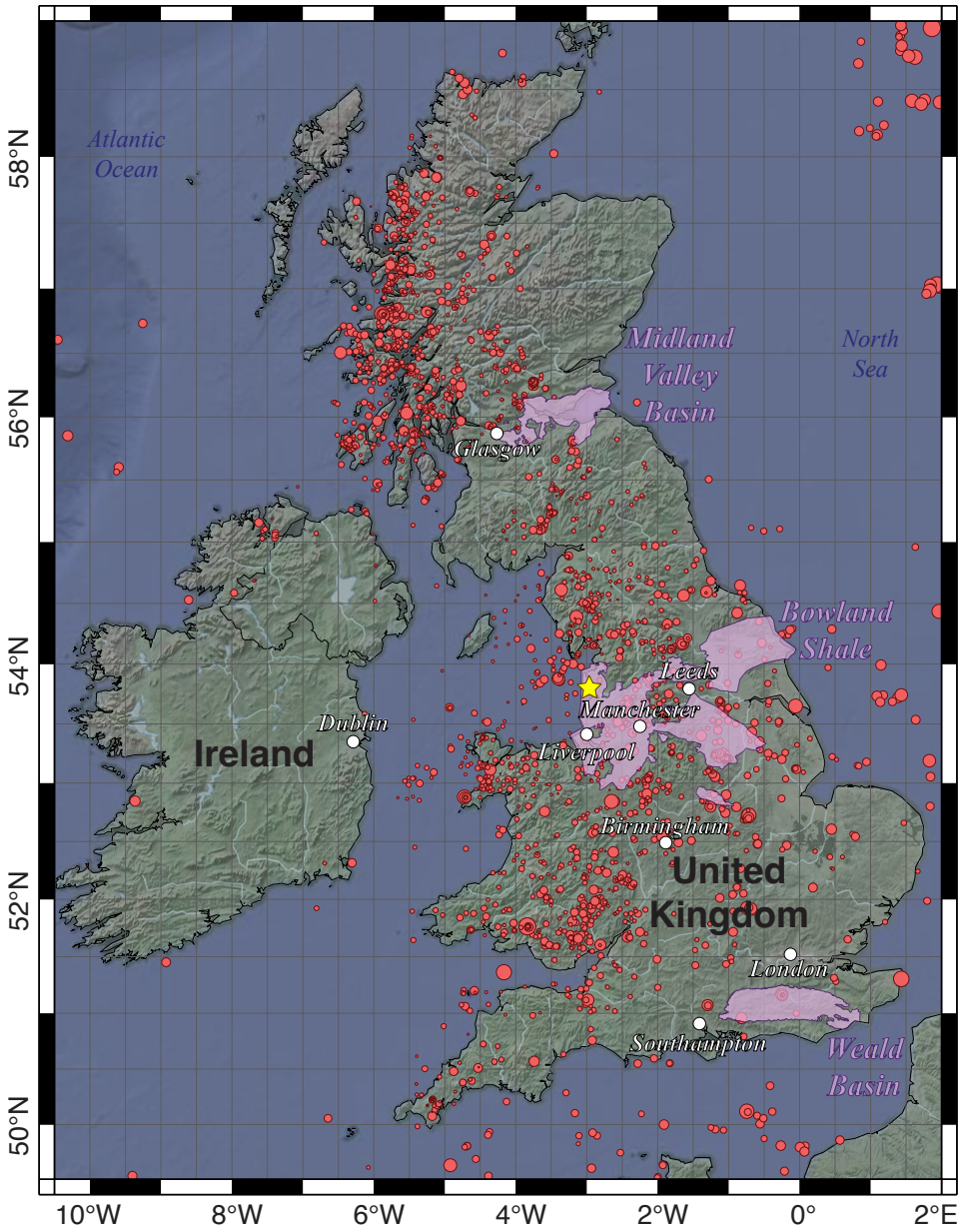

Figure 1 Map of the study area. Map of the UK including HF plays (purple polygons), HF wells (yellow star), earthquakes (red circles), and the largest municipalities (white circles).

lation at PH-1 during March-May of 2011 resulted in a series of induced earthquakes, the largest being the M_L 2.3 event on 1 April (de Pater and Baisch, 2011; Clarke et al., 2014). The induced events here were felt, leading to the suspension of the PH-1 operation, and an inquiry into the induced events (Green et al., 2012). The result of this inquiry was a regulatory roadmap that outlined monitoring requirements, seismic baseline assessment, fault avoidance strategies, mitigation measures, and a traffic light protocol (TLP) with a red-light threshold of M_L 0.5 (BEIS et al., 2013). Upon triggering a red-light, the operator must stop injection, reduce the pressure in the well, perform well integrity checks, and wait 18 hours before continuing stimulation (with regulatory approval).

A TLP is a regulatory control system designed with the intention of limiting the risks of induced seismicity (Majer et al., 2012). TLPs are typically designed with an escalating series of thresholds: green-light for unrestricted operation, yellow-light indicating when mitigation measures should be enacted, and the red-light for a regulatory intervention requiring the cessation of operation. Often (local) magnitude is used for delineating the yellow/red-light thresholds for practical reasons, like the simplicity of their estimation (Schultz et al., 2020a). The first case of a TLP used for induced seismicity hazard management was the Berlín geothermal project in El Salvador (Bommer et al., 2006). Since then, TLPs have been widely used for induced seismicity risk management (Ader et al., 2019; Schultz et al., 2020b) – including in the UK for HF.

The UK TLP was first put into a practical test in late-2018 with the Preston New Road 1z well (PNR-1z), targeting the Bowland Shale near Blackpool, Lancashire. HF operations at the PNR-1z well induced six events larger than M_L 0.5 that triggered the red-light, with the largest (M_L 1.6) event on 11 December 2018 being felt by some people nearby the epicentre (Clarke et al., 2019). Continuing nearly a year later (August 2019), the second

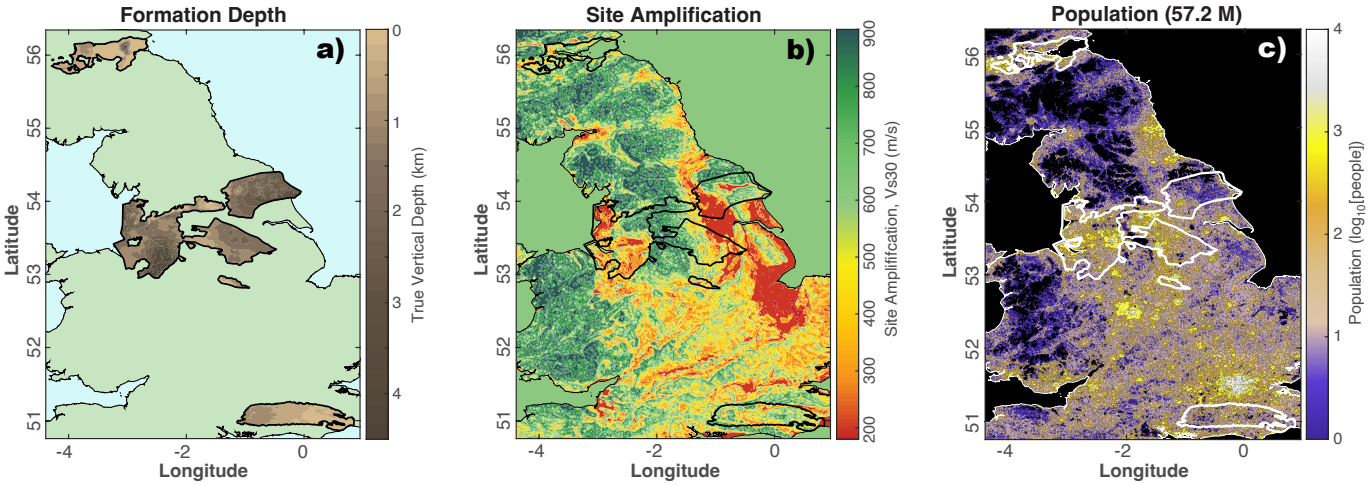

Figure 2 Maps of the input parameters for the UK. a) Depth contours for the target formation tops in the Midland Valley Basin, Bowland Shale, and Weald Basin (Andrews, 2013, 2014; Monaghan, 2014). b) Site amplification map, using slope-based V_{S30} as a proxy (Heath et al., 2020). c) Distribution of people throughout the UK (Rose et al., 2019). See also Figures S1, S2, & S3 for higher resolution versions.

lateral well (PNR-2) on the Preston New Road pad was hydraulically stimulated; the PNR-2 well also induced earthquakes, with the largest being M_L 2.9 on 26 August 2019. Notably, this event occurred more than 72 hours after the shut-in of the last stage (Kettlety et al., 2020) and was felt strongly near the epicentre (Edwards et al., 2021). This event led to the abandonment of this well, with only 7/47 planned stages being stimulated (Cuadrilla Resources Ltd, 2019). Consequently, this event triggered a review of the induced events (Oil and Gas Authority, 2018) and ultimately a moratorium on HF starting 2 November 2019. At the time of this study's publication the moratorium is ongoing.

Nevertheless, Russia's recent conflict against the Ukraine, and the knock-on effect of accompanying energy security needs in Europe, led the UK to reconsider their HF moratorium – prompting a report on recent HF induced seismicity understanding/management (Baptie et al., 2022). Previously, TLPs have been criticized for their inflexibility to consider events occurring after well shut-in and assumptions around the temporal sequence of largest magnitudes (Baisch et al., 2019). Since the UK moratorium, advancements have been made in understanding the earthquakes that follow well shut-in (Verdon and Bommer, 2020; Schultz et al., 2022a). As well, recent approaches have suggested translating seismic risks into equivalent red-light magnitude thresholds to better inform TLP designs (Schultz et al., 2020a, 2021a,b, 2022b).

In this study, we refine the *ad hoc* approaches of the past – instead, defining red-light thresholds using a risk-based approach. Like prior work, we find that risks vary spatially by orders of magnitude and that choosing a tolerance for risk allows for a fairer TLP design. In this case, we compare simulated risks from the 2019 PNR-2 M_L 2.9, 2.1, and 1.6 events to calibrate the UK tolerance for risk. These results indicate that red-light thresholds should vary from M_L 1.2-2.5, depending on exposure. Furthermore, we justify the importance of the risk metrics we considered and discuss their relevance for TLP design. Ultimately, a conscientious handling of induced seismicity risks will be important for the future of HF in the UK, especially considering the prior controversial history. Careful handling of HF risks will also be important for green energy development (like geothermal, carbon capture, or hydrogen storage), since 'perception spillover' can tarnish attitudes toward future industry (Westlake et al., 2023).

2 Data & Methods

Our TLP approach is based on risk evaluation and can be divided into three main categories: 1) determining the largest magnitude event following a HF operation, 2) estimating the resulting ground motion field, and 3) calculating the resulting seismic risks. Monte Carlo perturbations capture the variability within risk evaluations, which are repeated for all potential HF well locations in the UK (Figure 2). The details of each component are discussed in subsequent sections and have been described in previous works (Schultz et al., 2020a, 2021a,b, 2022b).

2.1 Trailing seismicity

Trailing seismicity refers to any earthquakes that occur after well injection stops. Sensitivity analysis has shown that these events are the most critical factor in designing a HF TLP (Schultz et al., 2021a). This is especially relevant, given that all the red-light events at the PNR-2 well occurred after stage stimulation was completed (Kettlety et al., 2020). Trailing magnitudes are estimated using a concept analogous to Båth's law (Båth, 1965), which states that the difference in magnitude between a mainshock and the largest aftershock ΔM depends on the count ratio R_S, the Gutenberg-Richter b-value, and confidence variables u_i (Schultz et al., 2022a).

$$\Delta M \approx \frac{1}{b}\log_{10}\left(\frac{1}{R_S}\right) + \frac{1}{b}\log_{10}\left(\frac{\ln(u_1)}{\ln(u_2)}\right) \quad (1)$$

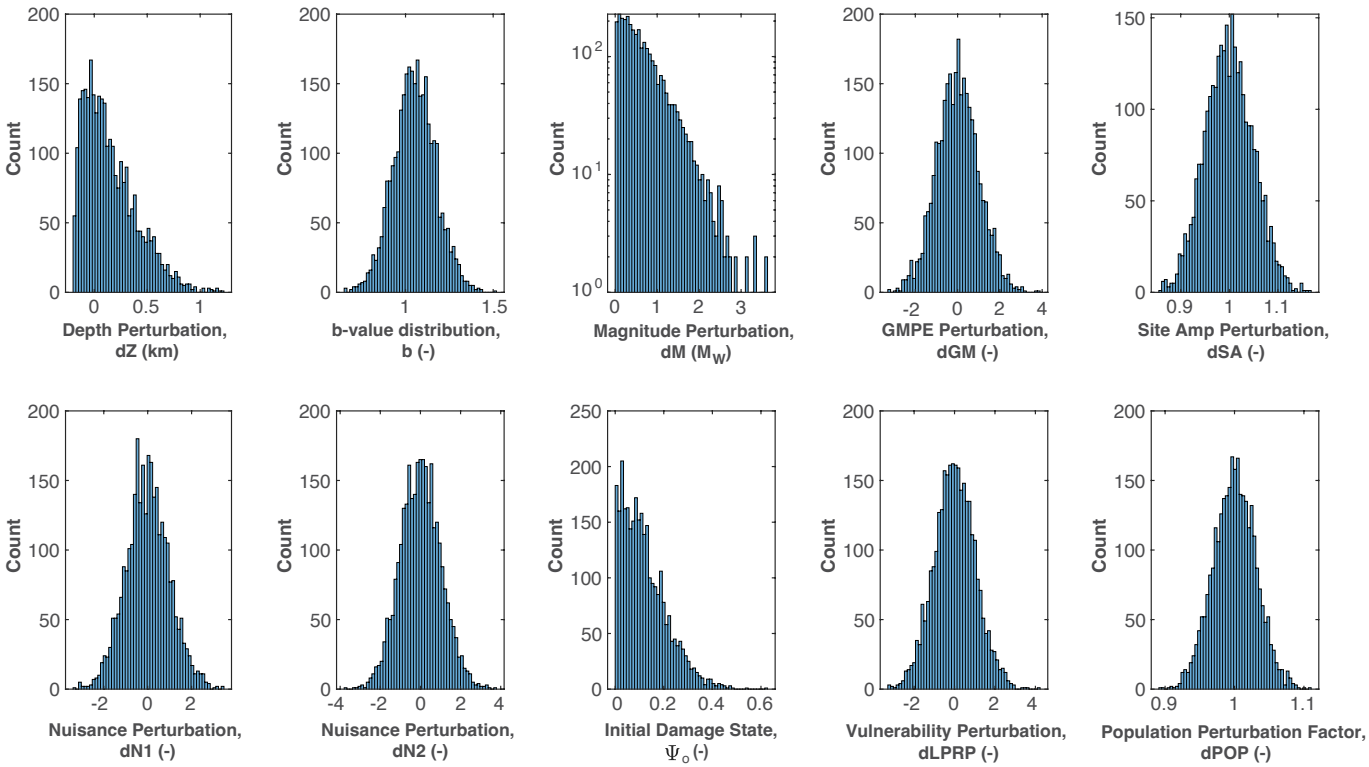

Figure 3 Perturbed input variables for the Monte Carlo analysis. Ten panels show histograms for each of the perturbed variables of interest: dZ – depth, b – *b*-value, dM – trailing magnitude, dGM – GMPE variability, dSA – site amplification perturbation factor, dN1 & dN2 – nuisance function variabilities, Ψ_o – initial damage state, dLPR – vulnerability function variability, and dPOP – population perturbation factor.

For the context of HF induced seismicity, we assume that a stimulation event (larger than the red-light) triggers a regulatory intervention that prompts well shut-in. Such an event is then followed by additional aftershock-like events trailing well shut-in. We inform our choice of *b*-value to be like those observed in the UK from various sources: prior tectonic seismicity baselines suggest values on the order of 1.01±0.06 (Mosca et al., 2022), while studies of the HF cases are closer to 1.10±0.10 (Kettlety et al., 2020) and 1.3 (Clarke et al., 2019). Each of these studies discerned significant variability in their *b*-values, depending on the subset of their data (Baptie et al., 2020). To encompass this range of *b*-values, we use a normal distribution with 1.05±0.12. The count ratio R_S represents the proportion of earthquakes occurring during stimulation to the total number of induced earthquakes. We use a distribution of R_S values based on the fit to the empirical data of short-term induced seismicity globally, like HF (Verdon and Bommer, 2020; Schultz et al., 2022a). This empirical R_S distribution has a mean and median value of 77% and 86%, respectively and was fit to a beta-distribution. As more information becomes available for induced seismicity caused by HF in the UK, this R_S distribution will be important to update as trailing seismicity is the most important factor in determining red-lights. In this sense, we can stochastically estimate the magnitude of the largest earthquake following a red-light (relative to the red-light) ΔM – by drawing random R_S and *b*-values from their distributions alongside uniform random values of u_1 and u_2. As well, we use a locally calibrated M_L-M_W conversion relationship (Edwards et al., 2021), a topic that has been extensively studied for the UK (Butcher et al., 2017; Luckett et al., 2018; Baptie et al., 2020; Roy et al., 2021). We refer readers to the prior study that details the statistical modelling of trailing earthquake magnitudes (Schultz et al., 2022a).

In addition to simulating the trailing event magnitudes, we also simulate the depth distribution of HF seismicity. The starting point for determining the depth is the top of the target formation, which provides the modal depth value and is based on geological assessments of shale targets in the UK. We use depths at formation tops to be conservative in our risk estimates. We consider the Limestone Coal Formation (Carboniferous) for the Midland Valley Basin (Monaghan, 2014), the Bowland Shale (Mississippian, Andrews, 2013), and the Kimmeridge Clay (Upper Jurassic) for the Weald Basin (Andrews, 2014, Figures 2a & S1). We do not account for UK legislation (UK Public General Acts, 2015) that prohibits HF operations shallower than 1000 m. We note that no exploration licenses have been awarded in Scotland, where a moratorium was imposed by the Scottish government in 2015. Additionally, no HF operations were completed in the Weald Basin. However, we include these basins to be comprehensive in our analysis and discussions. From the formation depth, the earthquakes are perturbed with a distribution that skews to deeper events (Figure 3). Typically, HF induced events occur near their stimulation interval, with some cases extending downwards into basement-rooted faults (Schultz et al., 2020b).

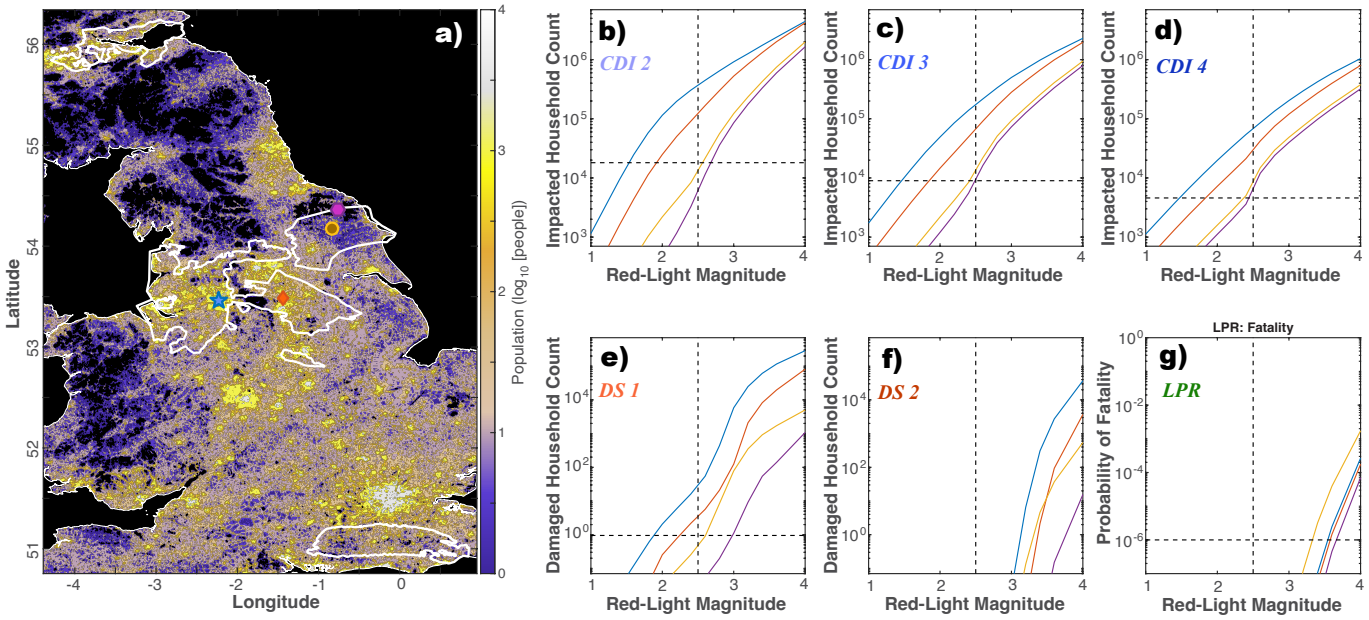

Figure 4 Risk curves for four locations. a) Population map of the UK showing the four locations sampled (coloured shapes) in the Bowland Shale. Median risk curves are plotted for nuisance at CDI 2 (b), CDI 3 (c), and CDI 4 (d) levels; damage at levels of DS 1 (e) and DS 2 (f); and LPR (g). Median risk curves are colour coordinated with their map locations. Iso-risk (horizontal dashed line) and iso-magnitude (vertical dashed line) are shown for reference.

2.2 Hazard Calculation

We use the simulated trailing earthquake scenarios to evaluate their hazards (Bommer, 2022) through a ground motion prediction equation (GMPE) – a formula that predicts the amplitude of earthquake ground motion based on factors such as magnitude, distance, depth, and site amplification. There are many GMPEs that are suitable for this region (Villani et al., 2019; Cremen et al., 2020), and we select one of them (Edwards et al., 2021). The effects of site amplification (Figures 2b & S2) are considered by using a global slope-based proxy for V_{S30} (Heath et al., 2020), corrected with non-linear NGA-West2 adjustments to the GMPE (Boore et al., 2014). The uncertainties in all inputs are perturbed via their standard errors, with ground motion also incorporating a spatially correlated intra-event error calibrated for European data (Esposito and Iervolino, 2012; Edwards et al., 2021). Our workflow primarily focuses on Peak Ground Velocity (PGV) as the key ground motion metric for nuisance and damage, but for building collapse assessment, we must use the geometric average of the spectral acceleration over various periods (Eads et al., 2015) – an important metric for assessing structural damage. The range of spectral acceleration periods averaged over (0.01s, 0.1s, 0.2s, 0.3s, 0.4s, 0.5s, 0.6s, 0.7s, 0.85s, & 1.0s) aligns with Groningen fatality risk studies (Crowley et al., 2017; Crowley and Pinho, 2020).

2.3 Risk Estimation

The estimated ground motion hazards are then translated into risk metrics like nuisance impacts, damage impacts, and chance of fatality. Risk metrics can be either aggregate (nuisance/damage) or local (individual chance of fatality). To compute the aggregate metrics, we use nuisance/fragility functions that define the chance of nuisance/damage as a function of ground motion (Figure S4). For this study, we use PGV-based North American nuisance functions (Schultz et al., 2021c) and Groningen fragility functions (Korswagen et al., 2019) to differentiate the degree of impact. Groningen fragility functions were chosen for their applicability to smaller to moderate magnitude (induced) seismicity, similar to prior studies in the UK (Edwards et al., 2021). For instance, degree of nuisance is categorized by Community Decimal Intensity (CDI, Wald et al., 2012) with levels ranging from 2-6 corresponding to subjective criteria of 'just felt', 'exciting', 'somewhat frightening', 'frightening', and 'extremely frightening', respectively. Similarly, the degree of damage is divided into damage states (DS, Korswagen et al., 2019), with levels 1-2 corresponding to visible light damage (>0.1 mm crack) and easily observable light damage (>1 mm crack), respectively. The third risk metric is a local risk that considers the chance of a specific type of fatality, known as local personal risk (LPR), which is the likelihood that a hypothetical person inside of a building for 95% of their time will suffer a building collapse death (SodM, Staatstoezicht op de Mijnen, 2014). To estimate this, we use the average Groningen vulnerability function (Crowley et al., 2017; Crowley and Pinho, 2020), which defines the chance of fatality as a function of period-averaged spectral acceleration. This vulnerability function is more conservative than the one used in PAGER's UK estimates (Figure S5) for global estimates of fatalities (Jaiswal et al., 2009; Caprio et al., 2015; Jaiswal and Wald, 2010). Our vulnerability and nuisance functions consider errors in these functions via a perturbation in their parameters (Figure S4), respectively (Figure 3). Our damage functions also include a building pre-damage term Ψ_o (Korswagen et al., 2019), which we assign a half Gaussian distribu-

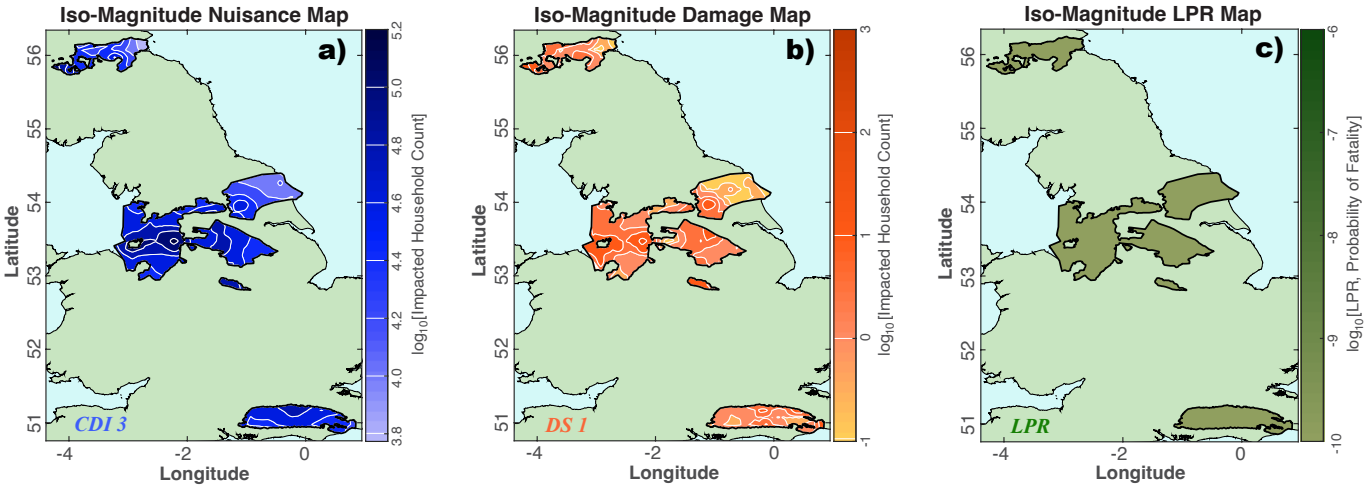

Figure 5 Iso-magnitude maps. a) Number of households impacted by CDI 3 nuisance. b) Number of households impacted by DS 1 damage. c) Map of LPR, the probability of loss of life. All maps use a red-light threshold of M_L 2.5. All maps have their risk metrics colored on a base-10 logarithmic scale. Damage and LPR maps are truncated at 10^{-1} and 10^{-10}, respectively.

tion (0.00+0.15) for perturbations (Figure 3). These error terms are included to account for uncertainties in estimating risk metrics via these simplified functions.

The severity of risk is then determined using an exposure model (Figures 2c & S3). The distribution of exposed population from the LandScan model (Rose et al., 2019) is gridded at ~1×1 km. Based on UK census data, we assume an average of 2.4 residents per household. The total number of homes affected by aggregate risk metrics is calculated by summing the expected number of homes affected at each 'shake grid' point (0.05×0.05°). As earthquakes of moderate magnitude have little to no far-reaching impact (Nievas et al., 2019), the simulation of nuisance and damage is limited to 400 and 40 km epicentral distance, respectively. The population maps are perturbed to account for variation in population distribution and uncertainties in our household inventory; each grid point is perturbed by a Poisson-like distribution (Gaussian with a mean of the grid point's value and a standard deviation of the square root of the value), to account for these uncertainties. LPR only considers the distance between the earthquake epicentre and the nearest populated grid point. When necessary, population is adjusted to reflect national temporal trends (Figure S6 U.N.-P.D., 2022).

2.4 Monte Carlo sampling

The final step is to account for the variabilities in individual components that will influence the output risk metrics. We use a 3000-trial Monte Carlo sampling approach in which all inputs are perturbed randomly via their previously described distributions (Figure 3). Inputs are sampled independently, with only nuisance parameter perturbations having a covariance (Schultz et al., 2021c). These repeated trials construct the statistical distribution of our risk metrics; by focusing on the median values, our red-light thresholds are the 50-50 chance of a given risk. We chose 3000-trials since this sample size produces stable median risk metrics estimates. For additional information on the workflow, we refer the reader to prior works on the subject (Schultz et al., 2020a, 2021a,b).

3 Results

With this approach (Section 2), we can now analyze the potential risk of HF cases in the UK. To do so, we begin by examining four test locations that are chosen to intentionally demonstrate the impact of exposure to our risk metrics (Figure 4). In each test location, risk increases monotonically as the red-light magnitude increases. However, the amount of risk in each location varies significantly for a constant red-light magnitude. We remind the reader that our approach quantifies the impacts that would happen following a red-light (including trailing seismicity) – it is unable to discern the likelihood of a red-light occurring, or the efficacy of an operator's mitigation procedures.

Our analysis begins by defining a single red-light threshold (*i.e.*, iso-magnitude) to examine how our three risk metrics vary with location. We then consider the impacts from prior UK HF seismicity to establish regional risk tolerances. Finally, we generate iso-risk maps that determine red-light thresholds based on these risk tolerances.

3.1 The iso-magnitude approach

First, we utilize our approach (Section 2) to determine the severity of risk for the geographic region of the UK. To do so, we create an 'earthquake grid' of 0.100×0.100° on which we simulate potential HF red-light earthquakes from a co-located HF operation. For each grid point, we assume a single red-light threshold of M_L 2.5. We choose this red-light threshold for two reasons: 1) this magnitude is below the 2019 M_L 2.9 PNR-2 earthquake and 2) this is slightly below the low end used for HF TLPs in North America (Schultz et al., 2021a). That said, we acknowledge that this choice is arbitrary.

Based on this premise, the impacts of our three estimated risk metrics (nuisance, damage, & LPR) are spatially heterogeneous and vary by orders of magnitude

Name/Place	Date	Magnitude (M_L)	Latitude	Longitude	Depth (km)	Tolerable?
HH-1	2019-02-27	3.2	51.160	-0.248	2.5	Intolerable
PNR-2	2019-08-26	2.9	53.787	-2.964	2.5	Intolerable
PH-1	2011-04-01	2.3	53.818	-2.950	2.3	Intolerable
PNR-2	2019-08-24	2.1	53.786	-2.969	2.1	Aggravating
PNR-2	2019-08-21	1.6	53.785	-2.971	2.1	Tolerable
PNR-1z	2018-12-11	1.6	53.787	-2.965	2.3	Tolerable

Table 1 Catalogue of the prominent (induced) events in the UK considered for our risk tolerance calibrations. See the text for a description on how event tolerability was chosen.

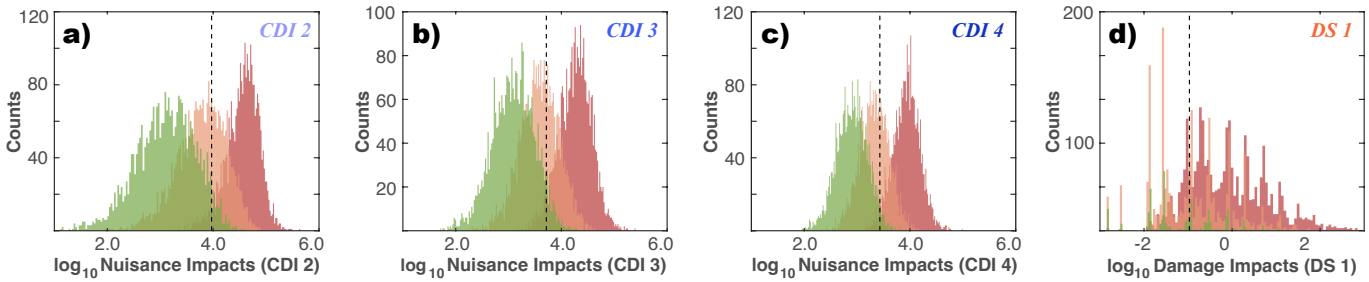

Figure 6 Modelled earthquake impact scenarios. Comparison of risk metrics between the M_L 1.6 (green bars), M_L 2.1 (orange bars) and M_L 2.9 PNR-2 events (red bars) alongside 50th percentile estimated tolerances for risk (dashed lines). Risk metrics of nuisance (a-c) and damage (d) are considered. All x-axis variables are in terms of the total number of homes impacted.

(Figure 5). The aggregate risk metrics (nuisance/damage impacts) follow the spatial population distribution, differing by their length scale. This difference in length scale has previously been explained by the typical range of damage/nuisance impacts for moderate magnitude earthquakes (*i.e.*, 10s/100s of kms, respectively). On the other hand, LPR appears to spatially correlate most strongly with the formation depth (Figures 2a & S1). This is because LPR is a local risk that we have estimated using the distance to the closest populated grid point. For the population distribution of the UK (Figures 2c & S3), effectively the epicentral distance is almost always 0 km, thus depth is effectively the only spatially varying input. This spatial variation in risk has previously been cited as a reason against iso-magnitude TLP designs (Schultz et al., 2021a,b).

3.2 Calibration of risk tolerances

In order to design fair TLPs, an iso-risk approach should be used. However, this approach requires making value-based decisions about acceptable risk tolerances, which can vary by region depending on the reputation of the operator and regulator (*i.e.*, the social license to operate, Smith and Richards, 2015; Thomas et al., 2017). To address this, we examine prior instances of HF-induced earthquakes in the UK to measure these tolerances empirically. We compare prominent (induced) earthquakes in the UK, that came under regulatory scrutiny (Table 1). For example, the HF induced events at PNR (Clarke et al., 2019; Kettlety et al., 2020) and PH-1 (Pater and Baisch, 2011; Clarke et al., 2014) are directly relevant for our study. We supplement this table with recent events near the Horse Hill well (HH-1), due to public concern (and regulatory scrutiny) that the events were induced hydrocarbon exploration. We emphasize that it is unlikely the Horse Hill earthquakes were induced (Hicks et al., 2019).

We use the known details of these events (Table 1) and a fit to the only free GMPE parameter (inter-event Z-score) based on observed shaking intensities. We do not use the trailing seismicity model in this case, since the event magnitude is known. From there, we proceed with the usual steps of our workflow, also utilizing 3000 Monte Carlo trials.

The estimation of the aggregate risk metrics is performed for all the significant (induced) events (Figures 6, S7, & S8). We separate the events into two bins: either having a tolerable or intolerable amount of risk, based on social/political reactions to the events. In this sense, we consider the M_L 2.9 PNR-2 event (and the Horse Hill or Preese Hall events) as the archetype of an intolerable amount of risk by UK standards, due to the public outrage and subsequent moratorium on HF development. The M_L 2.1 PNR-2 events are considered aggravating due to their public outrage and regulatory scrutiny, but operations were ultimately allowed to continue. All other events (Table 1) are considered tolerable (*e.g.*, M_L 1.6 PNR-2) because of a lack of social response (*e.g.*, regulatory change). Following this logic, we use these real events to 'bookend' UK tolerances to risks, by starting to constrain the upper/lower bounds to tolerances. For all three degrees of nuisance impacts (CDI 2-4), there is a clear separation between tolerable/intolerable event impacts (albeit with some overlap). For the damage impacts (DS 1-2), this separation is not as clear, with well-overlapping damage estimates from the three largest PNR-2 events.

From these observations, we begin to infer risk tolerances. We consider the intersection between the two PNR-2 (M_L 2.9 & 1.6) nuisance impacts as an empirical

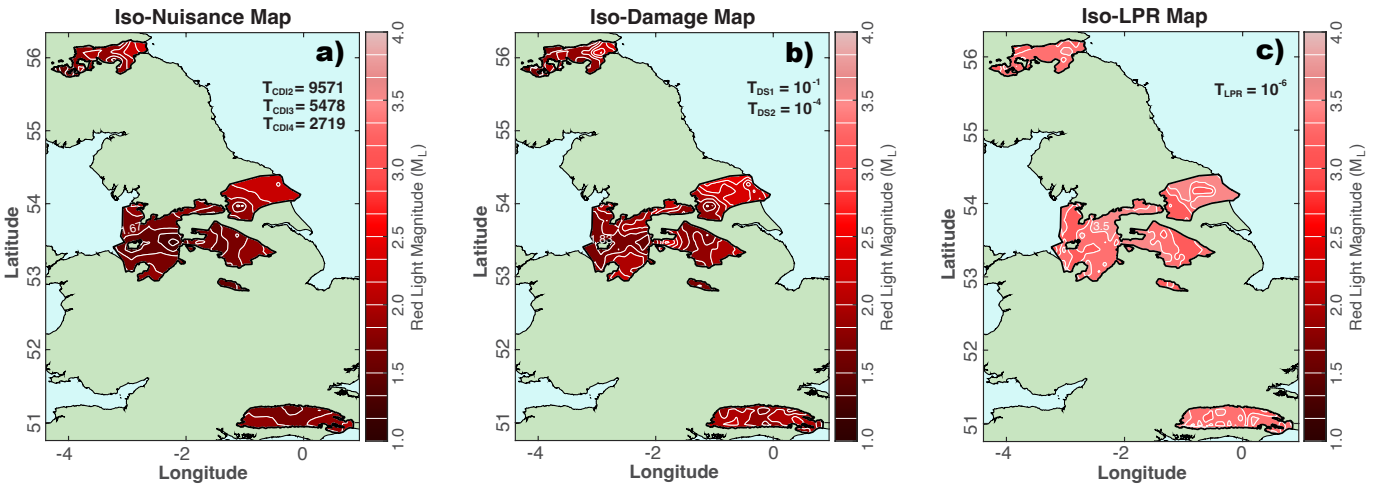

Figure 7 Iso-risk maps. a) Combination map of the three iso-nuisance maps (Figure S8). b) Combination map of the two iso-damage maps (Figure S9). c) Iso-LPR map. All maps have their tolerances for risk displayed as text.

measure of nuisance tolerance distribution. For damage tolerances, we consider the composite of the two PNR-2 damage impacts as an empirical measure of damage tolerance distribution. From these empirical tolerance distributions, we select the 50th percentile as our first choice for nuisance/damage tolerances. This 50th percentile choice results in nuisance tolerances roughly comparable to the modal/median value of the 2019 M_L 2.1 PNR-2 event (Figure 6). We note that estimates of tolerances from PNR-2 and PH-1 provide similar estimates (Figures 6 & S7), suggesting this approach is adequate for assessing a local populations tolerance to risks. Our 'bookending' approach estimated values of nuisance tolerance are T_{CDI2}=9571, T_{CDI3}=5478, T_{CDI4}=2719 impacted homes while damage tolerances are TDS1=10^{-1} and TDS2=10^{-4} impacted homes. Fatality risk tolerances are selected as 10^{-6} chance of occurring.

Last, we also provide a brief and qualitative comparison the 'Did You Feel it' reports collected by the British Geological Survey. Of all the earthquakes considered, we focus on the largest event (*i.e.*, the 2019 M_L 2.9 PNR-2 earthquake) which had 2266 submitted reports (*e.g.*, Edwards et al., 2021). Submitted reports indicated felt ground shaking intensities (EMS-98) of up to VI, although most are at V and IV; damage reports indicated 97 DS 1 and 50 DS 2 homes damaged. We emphasize that these felt/damage accounts are self-reported by the public, without expert verification. Our mean modelled values are 6249 CDI 2, 3298 CDI 3, and 1441 CDI 4 homes felt the event alongside 61 DS 1 and 0.01 DS 2 damaged homes. Taken at face-value, our modelled estimates of damage are approximately comparable to the reported values. We note that we intentionally use the modelled risk estimates of tolerance, rather than the reported metrics, to take advantage of estimation biases canceling out.

3.3 The iso-risk approach

We now apply an iso-risk approach using the empirically derived tolerances for aggregate risks in the UK (Section 3.2). Our tolerance for LPR is 10^{-6}, a conservative value for the range typically considered (Marzocchi et al., 2015; Commissie-Meijdam, 2015). Based on the previous risk curves (Section 3.1) and these risk tolerances, we then select red-light thresholds. We will discuss and justify the details and use of this risk tolerance later in the paper.

Prior research on nuisance has primarily focused on CDI 3, as tolerances to this metric are not well established (Schultz et al., 2021a,b). However, for the UK, we have empirically derived tolerances (Figures 6). We create separate iso-nuisance maps for each of the CDI 2-4 degrees (Figure S9). These individual maps are then combined into a single iso-nuisance map (Figure 7a), where the smallest red-light threshold from the three individual maps is selected at each grid point. In urban regions CDI 2 typically sets the threshold, while CDI 3 and CDI 4 control rural and remote regions, respectively (Figure S9). The differences between individual iso-nuisance maps are subtle, varying by no more than +0.4 M_L from the combination map. The iso-nuisance combination map has a spatial dependence on population distribution like the corresponding iso-magnitude map (Figure 5a).

We apply the same logic to the damage impacts risk metric, creating individual iso-damage maps that are then combined into a single iso-damage map (Figure S10). In this combined approach, the red-lights are entirely controlled by damage at the DS 1 level. It is worth noting that iso-damage combination exhibits a spatial dependence correlated with population distribution. The iso-damage map produces red-light thresholds that are roughly comparable to the iso-nuisance derived red-light thresholds.

Third, an iso-LPR map is produced using the same logic as the previous risk metrics (Figure 5c). Finally, we design TLP red-lights that will not exceed any of our risk metrics/tolerances by setting the smallest red-light threshold at each grid point (Figure 8). The median/mean values of this iso-risk combination map are M_L ~1.8, ranging between M_L 1.2-2.5, with 10th/90th percentiles at roughly M_L 1.6/2.2, respectively. When producing this combination map, nuisance and damage are roughly equivalent in concern (depending on location);

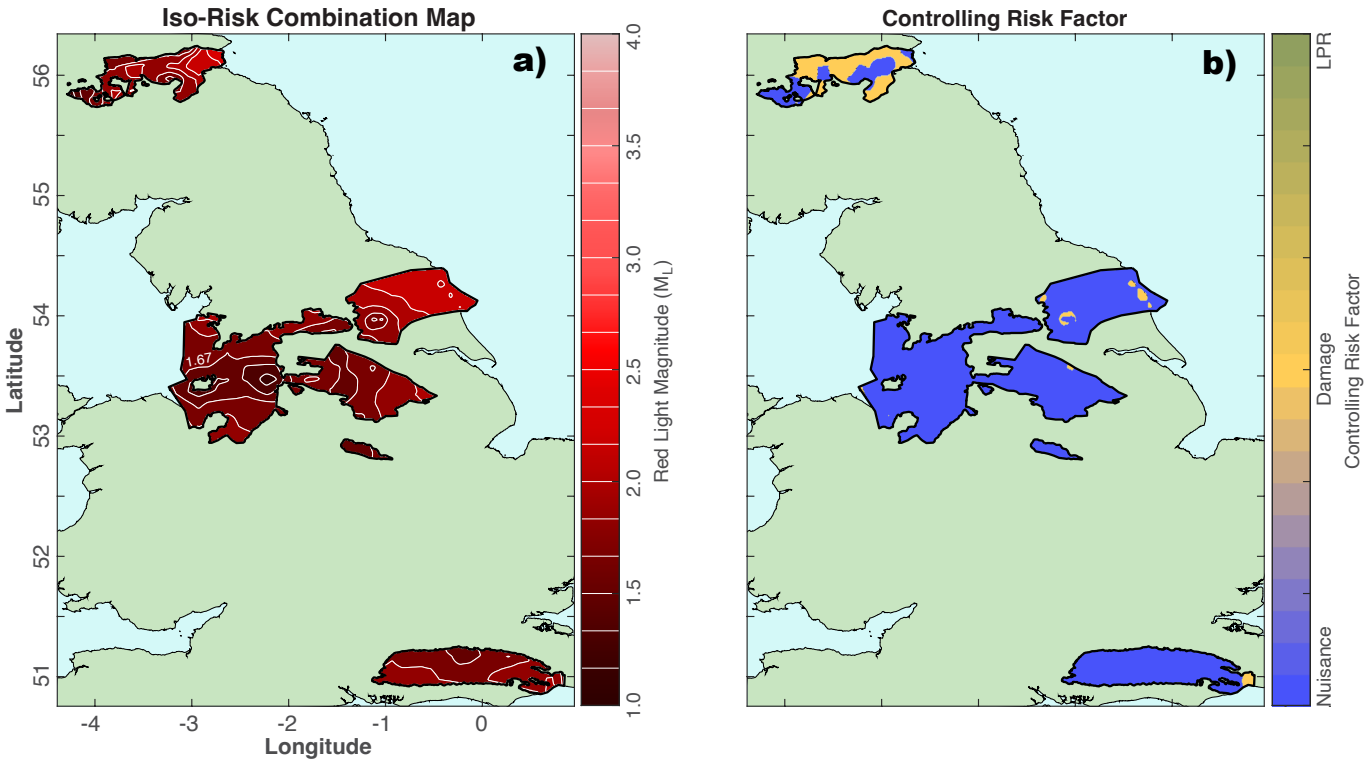

Figure 8 Combination map. a) Combination map of the three iso-risk maps (Figure 7). These three iso-risk maps are combined by taking the minimum red-light value at each grid point. b) Map showing which of the three iso-risk maps was the minimum red-light value for each grid point.

although, both nuisance and damage completely eclipse LPR concerns (Figure 8b).

4 Discussion

We discuss our results and their implications for effective TLP design in the UK.

4.1 Justification of risk metrics & risk tolerance choices

Here we briefly justify the use of our risks metrics and the tolerances derived for each metric. The use of LPR is much more straightforward than the other risks: there is an obvious need to keep citizens safe from harm and guidelines on tolerances to this risk (10^{-6}-10^{-4}) already exist, both for tectonic earthquakes (Marzocchi et al., 2015) and induced earthquakes (Commissie-Meijdam, 2015). This concern is relevant, since losses, both human and economic, have already resulted from HF induced earthquakes (Lei et al., 2019).

The inclusion of damage risks is also important, considering the aforementioned cases of damage. However, the exact handling of damage (and their tolerances) isn't quite as clear. One example is the Dutch handling of damage, where residents are entitled to compensation following a formal report and verify process – although there is a general feeling among the population that this handling is inadequate (van der Voort and Vanclay, 2015). In the case of the UK, our estimates suggest that residents are unwilling to accept any amount of damage, even at the DS 1 level (Figure 6d). This empirical estimate of damage tolerance has a tidy correspondence with the UK regulator's mandate, which is to "minimize the number of events felt at the surface by the public and to avoid the possibility of events capable of causing damage to nearby buildings or infrastructure" (Clarke et al., 2019; Oil and Gas Authority, 2018). Based on this information, we feel justified in our choice of (conservative) damage risk tolerances.

The inclusion of nuisance is the most nebulous risk metric: both because of the lack of prior consideration and predefined tolerances. Despite these limitations, previous 'good practice' guidelines have discussed the importance of nuisance (Majer et al., 2012) and legal frameworks often have liabilities defined around nuisance (Cypser and Davis, 1998). Building on this, many HF cases of regulatory intervention (*i.e.*, enacting a TLP, triggering a red-light, or ending the operation) have occurred without reports of damage or fatality (Schultz et al., 2021a,b). Furthermore, other studies on HF induced earthquakes in the UK have also highlighted the importance of quantifying/modelling nuisance (Cremen and Werner, 2020). Together, these points justify the inclusion of nuisance risks. The next step is to adequately choose nuisance tolerances. The definition of the red-light is the last-possible stopping-point before exceeding a tolerance to risk – *i.e.*, abandoning the operation to prevent taking an unacceptable risk. Based on this rationale, we have defined our nuisance tolerance to be between events that did/didn't trigger operation-ending regulatory interventions (Figure 6). In this sense, our selected nuisance tolerance threatens to end an operation (regardless of the existence of a predefined red-light). Last, we check these

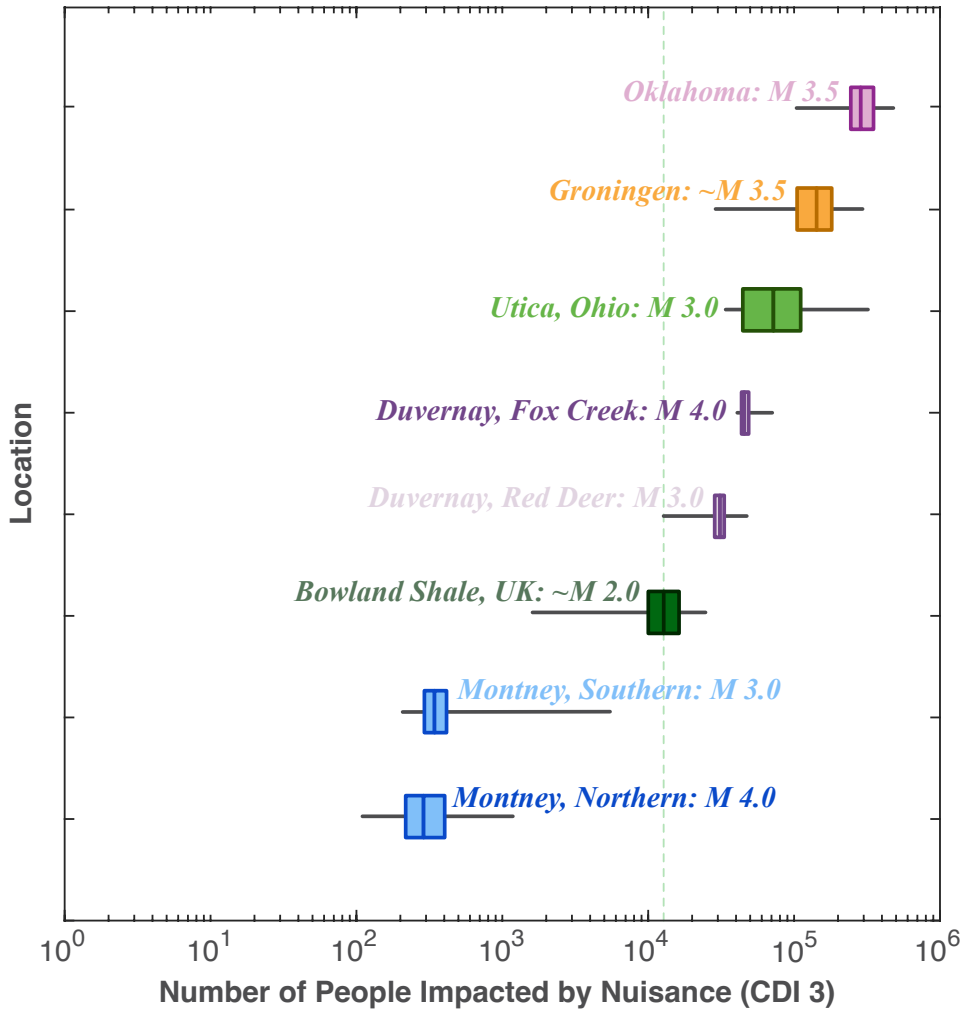

Figure 9 Worldwide nuisance tolerance estimates. The distribution of CDI 3 nuisance tolerance (box-and-whisker plots; boxes show 25-50-75 percentiles) for the UK (Figure 6) is compared to estimates in North America and the Netherlands (Schultz et al., 2021b, 2022b). The 50th percentile of the nuisance tolerance distribution, used to select the nuisance tolerance, is shown as green dashed line.

empirically derived nuisance tolerances against other measured tolerances (Figure 9, Schultz et al., 2022b, 2021b). We find that UK tolerances to nuisance are most like the risks implicitly taken by TLPs in Alberta, despite the significantly different red-light magnitude thresholds chosen there (*i.e.*, M_L 3.0 near Red Deer and M_L 4.0 near Fox Creek). Based on this, we feel that our inclusion of nuisance within the red-light design is justified. We note, however, that this approach can easily be repeated/updated using different tolerances as new information becomes available.

These tolerances result in red-light thresholds that vary spatially between M_L 1.2-2.5 (Figure 8). Comparatively, our thresholds are much smaller than the magnitudes of the largest recorded tectonic events onshore (M_L ~5) or offshore (M_L ~6, Musson, 2007, 2004) and smaller still than prior coal mining (M_L 3.1, Redmayne, 1988; Redmayne et al., 1998) or potash mining (1989 M_L 2.4, Browitt, 1991; Wilson et al., 2015) induced seismicity. These induced events were tolerated by the public, over a period of decades and in regions coincident with shale gas basins (Wilson et al., 2015). Cursory examination of temporal population trends (Figure S6, U.N.-P.D., 2022) suggests growth of ~10-20% since 1980, which can't account for the disparity between our red-lights and the previously accepted magnitudes. Similarly, our estimates of risk tolerances for the Horse Hill events (initially suspected as extraction-related, but found to be tectonic, Hicks et al., 2019) suggest tolerances approximately an order of magnitude larger than the ones derived for HF in the UK. We argue that these observations are not contradictory. Local tolerances are influenced by factors such as the type of risk, familiarity with the risk, consent to risk, geopolitical zeitgeist, personal needs, and past experiences (Marzocchi et al., 2015). In fact, surveys conducted in the UK indicate that local population are far less tolerant of earthquakes caused by HF compared to any other resource exploitation techniques (Evensen et al., 2022), supporting the differences of our tolerance estimates between HF and conventional hydrocarbon extraction (Figures 6, S7 & S8). If anything, this observation demonstrates the importance of maintaining a 'social license to operate' through effective outreach and communication (Majer et al., 2012).

In general, it is important to consider a combination

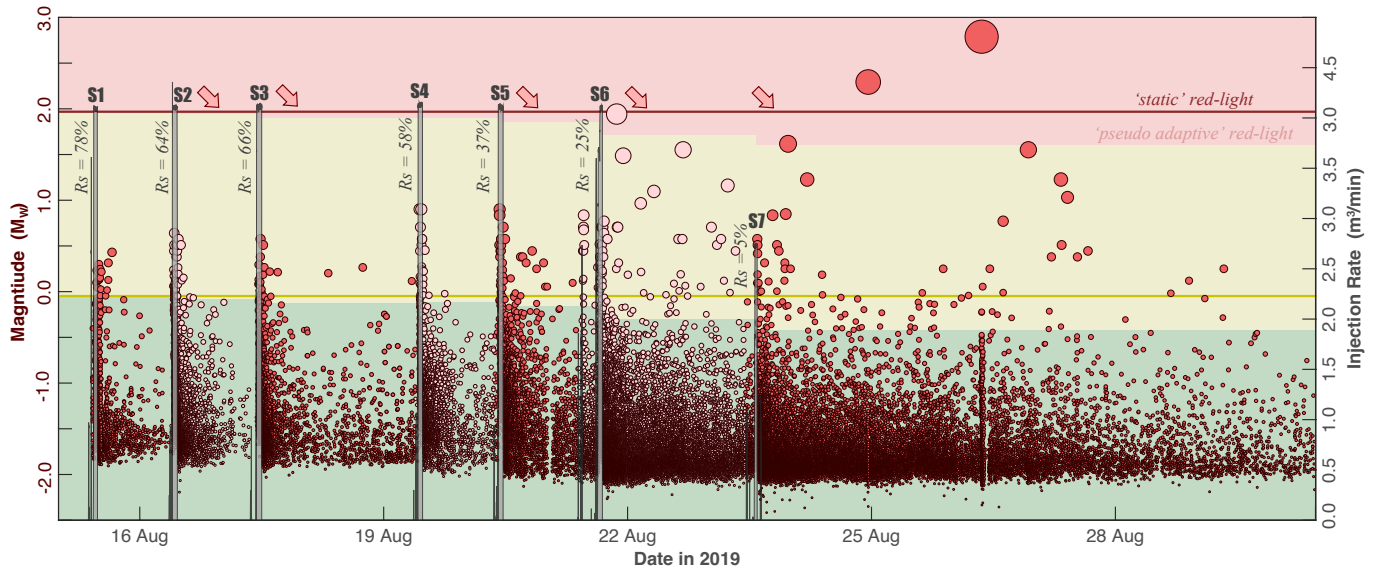

Figure 10 The proposed TLP retrospectively applied to PNR-2. Stimulation operations (grey areas) for the first seven stages (text labels) are shown alongside the induced earthquakes (red circles) and our proposed TLP thresholds: both 'static' *a priori* thresholds (solid-coloured lines) and 'pseudo adaptive' thresholds (coloured background) based on information from the previous stage stimulation. Red arrows indicate stages when the adaptive TLP red-light threshold sequentially decreases. Red-light moment magnitudes were estimated using an M_L-M_W conversion relationship (Edwards et al., 2021).

of all the risk metrics mentioned. Our approach offers the advantage of being able to simply combine multiple risk metrics (such as nuisance, damage, and fatality) and types (local or aggregate) by translating them into red-light thresholds. After defining the red-light, we can also link the design of yellow-light thresholds (Schultz et al., 2020a). Yellow-lights serve as a signal for operators to take appropriate mitigation measures before reaching the red-light threshold. However, magnitude 'jumps' (Verdon and Bommer, 2020) could create green-to-red transitions, rendering the yellow-light ineffective. Hence, setting an appropriate gap between yellow- and red-light thresholds is crucial to prevent this from happening. Previous studies (Schultz et al., 2020a) have suggested that yellow-light thresholds 2.0 magnitude units lower than the red-light is sufficient, although this depends on a jurisdiction's tolerance for triggering red-lights.

4.2 Retrospective comparison with the prior UK TLP

Our workflow enables a comparison with the prior TLP for the UK, which had a red-light set at M_L 0.5 that included an 18 hour pause (BEIS et al., 2013). Importantly, this differs from our definition of an operation-ending regulatory intervention for the red-light. By our standard, the prior UK 'red-light' is better defined as a yellow-light with prescriptive mitigation. In the location of the PH-1 well (Pater and Baisch, 2011; Clarke et al., 2014), which initially triggered the enactment of the prior TLP, our analysis suggests a red-light threshold of M_L ~1.7. If the aforementioned (Section 4.1) 2.0 magnitude gap between red-yellow is taken for a new TLP, this would indicate a yellow-light threshold of M_L -0.3, which is more conservative than the prior value of M_L 0.5. If we instead considered the old threshold as a proper red-light, we estimate that this scenario would only be weakly felt (CDI 2) at 10s of homes.

Our results also facilitate a retrospective analysis against known cases of HF induced earthquakes. In particular, the PNR-2 case is most relevant due to the 2019 M_L 2.9 event which prematurely ended operations (Kettlety et al., 2020). In this location, our results suggest a red-light threshold of M_L ~1.7. From the time history of events in this location, this red-light threshold would not have been triggered before the seventh (and final) stage of stimulation; the 26 August 2019 M_L 2.9 event occurred more than 72 hours after the completion of stage seven (Figure 10). The third largest event, which was induced from the sixth stage stimulation (21 August 2019 M_L 1.6), falls just below our red-light threshold (M_L 1.7). Following a similar comparison, our red-light thresholds would have been triggered for PH-1 (following the 2011 M_L 2.3 event) and would not have been triggered for PNR-1z (Figures S11 & S12) – as intended by our tolerance definitions.

The PNR-2 case highlights the need for updating of 'static' or *a priori* red-lights with incoming real-time information. Specific to PNR-2, we would expect that the red-light should decrease with time: the first six stages showed an anomalously high proportion of trailing seismicity (R_S=48%) compared to the global average (~86%) used to define our red-light (Schultz et al., 2020b, 2022a). Importantly, R_S is the most influential parameter for varying red-light thresholds (Schultz et al., 2021a). Similarly, the stage completions at PNR-1z (R_S=41%) and PH-1 (R_S=46%) also have a large proportion of trailing events compared to global averages (Schultz et al., 2022a). These systematically low values of R_S at PNR-1z and PNR-2 can explain the significant trailing seismicity observed for each well stage. Because of these trailing seismicity observations, we would expect that a dynam-

ically updated red-light would have decreased from our static value as operations progressed.

To roughly demonstrate these dynamic red-light changes, we perform a pseudo adaptive update in response to the PNR-2 catalogue (Figure 10). Our simplistic approach assumes a change in the red-light threshold based entirely on the change of R_S value from the previous stage: essentially, we draw 10^6 trailing/red-light events for a given value of R_S , compute the median ΔM, and update the red-light in comparison to the difference from the global *a priori* median ΔM. This pseudo adaptive approach also demonstrates the sensitivity of red-lights to R_S changes. For example, stages five and six observed deviant R_S values of 37% and 25%, which reduce the red-light of subsequent stages by ~0.2 and ~0.4 M_W units (from the static red-light value), respectively. This simple updating process would have triggered a red-light following the 21 August 2019 M_L 1.6 event of stage six at PNR-2, ultimately ending the operation before the larger events of stage seven. Interestingly, this same process applied to PNR-1z still does not trigger a red-light, which is the intended goal for this case (Figure S11). Unfortunately, there are insufficient seismological data at the PH-1 case to adequately perform our pseudo adaptive TLP approach, so we are unable to assess if the M_L 2.3 event could have been avoided (Figure S12). Of course, this analysis has the benefit of hindsight; in practice, it is not well established how nearby stages are connected to seismogenic faults, linked in seismic response, and how well measured parameters (like R_S) would translate between stages – or how to forecast any of these considerations. While implementing a more rigorous updating of red-light values is beyond the scope of this paper (*e.g.*, Mignan et al., 2017), the HF events at PNR-2 appear to be an ideal case to test and develop this type of approach.

4.3 Prospective HF site recommendations

The design of a risk-based TLP for the UK provides a unique opportunity to begin discussing safer HF siting locations. The contentious history of HF in the UK (Williams et al., 2016) and induced earthquakes (Baptie et al., 2022) certainly makes this a significant concern. All of the basins have similar average risks (mean red-lights of M_L ~1.8); however, the Weald Basin (Figures 5, 7 & 8) is the most homogeneous, only ranging between M_L 1.6-2.0. The Bowland Shale has more disparate range M_L 1.2-2.3. The Midland Valley Basin has the most disparate ranges of red-lights, M_L 1.2-2.5 – largely due to the waterscapes where the Firth of Forth connects to the North Sea, near Edinburgh.

However, induced seismicity is not the only consideration: the anticipated productivity and the logistics/-costs of a prospective location also play a significant role in siting HF wells. The Bowland Shale has been considered the most prospective basin (Smith et al., 2010; Andrews, 2013), with operations targeting the western coast near Blackpool and Preston (e.g, PH-1, PNR-1z, & PNR-2 in Figure 1). These locations have red-light values near M_L 1.7, which is a location with slightly below average risk (owing to exposure). Highest risks are within the ~20 km vicinity of Manchester (M_L ~1.3), Liverpool, and York. The lowest Bowland Shale risks (M_L 2.3) are in a wide area near the eastern coast, from Bridlington to Scarborough. Depending on trade-offs for reduced productivity and logistical costs, this region could be a safer site choice (from the perspective of induced seismicity risks). Overall, our iso-risk red-light maps (Figure 8) facilitate comparisons and could be used to site prospective HF operations in the UK. We note that this approach focuses solely on the potential exposure to risks. Complementary siting approaches that consider the likelihood of induced seismicity, depending on the geological susceptibility to earthquakes (Pawley et al., 2018; Hicks et al., 2021), could also aid in choosing safer HF locations.

4.4 Limitations of our model and results

In this section, we briefly cover the limitations imposed by our model and the derived results. Firstly, components of our approach are based on models that were translated from other cases (*e.g.*, Groningen fragility and vulnerability functions). If more HF induced earthquakes occur, our model should be refined and updated accordingly. We want to emphasize that our workflow is adaptable and can incorporate new components or updates as needed. For example, if potential HF induced earthquakes in the UK are found to be only limited to a susceptible geographic region, a more targeted approach that utilizes known building inventories could improve risk assessments (Edwards et al., 2021). As well, risks posed to critical infrastructure could be included in the red-light determination, in relevant regions.

Our analysis has focused on the median risk values: *i.e.*, the 50-50 chance of a given risk impact. However, mean values are more informative being the expected risk impact. Our risk metrics have a heavy-tailed distribution, implying that the mean values will be strongly influenced by rare, high-consequence events with small likelihood. Therefore, using mean values instead of median would result in lower red-light thresholds. To better constrain these distributions, we would need a regional calibration of trailing count ratios (R_S), a better understanding of the maximum possible magnitudes, and component models that can extrapolate within appropriate ranges.

Finally, our approach has assumed static tolerances to risk, where a population suddenly changes their stance after risk value has been surpassed. Largely, this is due to the limited amount of data available to calibrate risk tolerances – our 'bookending' approach can only infer a range of values that the tolerance lies between. In reality, these tolerances may be time-dependent: such as by diurnal differences in tolerance, influenced by cumulative impacts from an operation, varying as the social license adjusts, or in response to growing urbanization/population increasing the amount of asset exposure. Much of our tolerance constraining approach has been restricted by the limitations of data/-case availability to make empirical inferences. To improve on these limitations would require methodologi-

cal improvements for tolerance estimation, conceptual advances in modeling social change, or policy direction that explicitly defines agreeable risk tolerances.

5 Conclusions

To manage hypothetical induced seismicity in the UK, we have employed a risk-based design of TLP red-lights. We have relied on previously developed seismic hazard and risk research for the HF in the UK and the Groningen gas field (as a reasonable analogue). By contrasting the M_L 2.9, 2.1, and 1.6 PNR-2 events, we were able to empirically calibrate the UK tolerances to nuisance and damage risks. These calibrated tolerances are comparable to those established for HF in North America. Our findings indicate that nuisance and damage impacts impose more stringent red-lights than LPR. Based on our red-lights, we suggest potential sites where prospective HF wells could be drilled. The integration of these three risk metrics (nuisance impacts, damage impacts, and LPR) provides a quantitative basis for reference red-light thresholds to inform future HF TLPs in the UK, should the current moratorium be lifted. These results can also be adapted for other greener industries such as deep geothermal energy or carbon/hydrogen storage.

Acknowledgements

We would like to thank James Verdon and an anonymous reviewer for their critiques that helped improve this manuscript and Stephen Hicks for handling our manuscript as the editor. Grammatical editing of our manuscript was assisted by ChatGPT.

Data and code availability

Formation depths (Andrews, 2013, 2014; Monaghan, 2014), trailing seismicity model (Schultz et al., 2022a), GMPE model (Edwards et al., 2021), spatial noise correlation model (Esposito and Iervolino, 2012), site amplification (Heath et al., 2020), population density (Rose et al., 2019), nuisance function (Schultz et al., 2021c), fragility function (Korswagen et al., 2019), and vulnerability function (Crowley et al., 2017; Crowley and Pinho, 2020) are derived from prior studies. Earthquake catalogues and felt/damage reports are available online (https://earthquakes.bgs.ac.uk/earthquakes/dataSearch.html, https://www.nstauthority.co.uk/exploration-production/onshore/onshore-reports-and-data/preston-new-road-well-pnr2-data-studies/ & https://www.nstauthority.co.uk/exploration-production/onshore/onshore-reports-and-data/preston-new-road-pnr-1z-hydraulic-fracturing-operations-data/). Routines and publicly available data used to create the figures and results of this paper can be found online at GitHub https://github.com/RyanJamesSchultz/TLPuk or at Zenodo (https://doi.org/10.5281/zenodo.8416391). Additional materials on the workflow are also discussed in prior studies (Schultz et al., 2021a,b, 2022b).

Competing interests

The authors declare no competing interests.

References

Ader, T., Chendorain, M., Free, M., Saarno, T., Heikkinen, P., Malin, P. E., Leary, P., Kwiatek, G., Dresen, G., Bluemle, F., and Vuorinen, T. Design and implementation of a traffic light system for deep geothermal well stimulation in Finland. *Journal of Seismology*, 24(5):991–1014, Aug. 2019. doi: 10.1007/s10950-019-09853-y.

Andrews, I. The Carboniferous Bowland Shale gas study: geology and resource estimation. *British Geological Survey for Department of Energy and Climate Change*, page 64, 2013.

Andrews, I. The Jurassic shales of the Weald Basin: geology and shale oil and shale gas resource estimation. *British Geological Survey for Department of Energy and Climate Change*, page 89, 2014.

Atkinson, G. M., Eaton, D. W., Ghofrani, H., Walker, D., Cheadle, B., Schultz, R., Shcherbakov, R., Tiampo, K., Gu, J., Harrington, R. M., Liu, Y., van der Baan, M., and Kao, H. Hydraulic Fracturing and Seismicity in the Western Canada Sedimentary Basin. *Seismological Research Letters*, 87(3):631–647, Mar. 2016. doi: 10.1785/0220150263.

Atkinson, G. M., Eaton, D. W., and Igonin, N. Developments in understanding seismicity triggered by hydraulic fracturing. *Nature Reviews Earth & Environment*, 1(5):264–277, May 2020. doi: 10.1038/s43017-020-0049-7.

Baisch, S., Koch, C., and Muntendam-Bos, A. Traffic Light Systems: To What Extent Can Induced Seismicity Be Controlled? *Seismological Research Letters*, 90(3):1145–1154, Mar. 2019. doi: 10.1785/0220180337.

Baptie, B., Luckett, R., Butcher, A., and Werner, M. Robust relationships for magnitude conversion of PNR seismicity catalogues. *British Geological Survey Open-File Report*, 20(042):32, 2020.

Baptie, B., Segou, M., Hough, E., and Hennissen, J. Recent scientific advances in the understanding of induced seismicity from hydraulic fracturing of shales. *British Geological Survey Open Report*, 22(050):51, 2022.

Båth, M. Lateral inhomogeneities of the upper mantle. *Tectonophysics*, 2(6):483–514, Dec. 1965. doi: 10.1016/0040-1951(65)90003-x.

BEIS, D. f. B., Energy, and Strategy, I. Regulatory Roadmap: Onshore oil and gas exploration in the UK regulation and best practice, 2013. https://www.gov.uk/government/publications/regulatory-roadmap-onshore-oil-and-gas-.

Bickle, M., Goodman, D., Mair, R., Roberts, J., Selley, R., Shipton, Z., and Younger, P. Shale gas extraction in the UK: a review of hydraulic fracturing. In *The Royal Society and The Royal Academy of Engineering Report*, page 76. 2012.

Bommer, J. J. Earthquake hazard and risk analysis for natural and induced seismicity: towards objective assessments in the face of uncertainty. *Bulletin of Earthquake Engineering*, 20(6):2825–3069, Apr. 2022. doi: 10.1007/s10518-022-01357-4.

Bommer, J. J., Oates, S., Cepeda, J. M., Lindholm, C., Bird, J., Torres, R., Marroquín, G., and Rivas, J. Control of hazard due to seismicity induced by a hot fractured rock geothermal project. *Engineering Geology*, 83(4):287–306, Mar. 2006. doi: 10.1016/j.enggeo.2005.11.002.

Boore, D. M., Stewart, J. P., Seyhan, E., and Atkinson, G. M. NGA-West2 Equations for Predicting PGA, PGV, and 5% Damped PSA for Shallow Crustal Earthquakes. *Earthquake Spectra*, 30(3):1057–1085, Aug. 2014. doi: 10.1193/070113eqs184m.

Browitt, C. UK Earthquake Monitoring 1989/90. *British Geological Survey Technical Report WL/SO/13*, page 36, 1991.

Butcher, A., Luckett, R., Verdon, J. P., Kendall, J.-M., Baptie, B., and Wookey, J. Local Magnitude Discrepancies for Near-Event Receivers: Implications for the U.K. Traffic-Light Scheme. *Bulletin of the Seismological Society of America*, 107(2):532–541, Jan. 2017. doi: 10.1785/0120160225.

Caprio, M., Tarigan, B., Worden, C. B., Wiemer, S., and Wald, D. J. Ground Motion to Intensity Conversion Equations (GMICEs): A Global Relationship and Evaluation of Regional Dependency. *Bulletin of the Seismological Society of America*, 105 (3):1476–1490, May 2015. doi: 10.1785/0120140286.

Clarke, H., Eisner, L., Styles, P., and Turner, P. Felt seismicity associated with shale gas hydraulic fracturing: The first documented example in Europe. *Geophysical Research Letters*, 41 (23):8308–8314, Dec. 2014. doi: 10.1002/2014gl062047.

Clarke, H., Verdon, J. P., Kettlety, T., Baird, A. F., and Kendall, J.-M. Real-Time Imaging, Forecasting, and Management of Human-Induced Seismicity at Preston New Road, Lancashire, England. *Seismological Research Letters*, July 2019. doi: 10.1785/0220190110.

Commissie-Meijdam. Eindadvies Handelingsperspectief voor Groningen Ad- viescommissie 'Omgaan met risico's van geïnduceerde aardbevingen', 2015.

Cremen, G. and Werner, M. J. A novel approach to assessing nuisance risk from seismicity induced by UK shale gas development, with implications for future policy design. *Natural Hazards and Earth System Sciences*, 20(10):2701–2719, Oct. 2020. doi: 10.5194/nhess-20-2701-2020.

Cremen, G., Werner, M. J., and Baptie, B. A New Procedure for Evaluating Ground-Motion Models, with Application to Hydraulic-Fracture-Induced Seismicity in the United Kingdom. *Bulletin of the Seismological Society of America*, 110(5):2380–2397, Mar. 2020. doi: 10.1785/0120190238.

Crowley, H. and Pinho, R. Report on the Fragility and Consequence Models for the Groningen Field (Version 7, 2020. https://nam-onderzoeksrapporten.data-app.nl/reports/download/groningen/en/9d8819b7-f0c5-4089-a036-71e755fda328. URL:.

Crowley, H., Polidoro, B., Pinho, R., and van Elk, J. Framework for Developing Fragility and Consequence Models for Local Personal Risk. *Earthquake Spectra*, 33(4):1325–1345, Nov. 2017. doi: 10.1193/083116eqs140m.

Cuadrilla Resources Ltd. Hydraulic Fracture Plan PNR 2, URL, 2019. https://consult.environment-agency.gov.uk/onshore-.

Cypser, D. A. and Davis, S. D. Induced seismicity and the potential for liability under U.S. law. *Tectonophysics*, 289(1-3):239–255, Apr. 1998. doi: 10.1016/s0040-1951(97)00318-1.

Eads, L., Miranda, E., and Lignos, D. G. Average spectral acceleration as an intensity measure for collapse risk assessment. *Earthquake Engineering & Structural Dynamics*, 44(12):2057–2073, Mar. 2015. doi: 10.1002/eqe.2575.

Edwards, B., Crowley, H., Pinho, R., and Bommer, J. J. Seismic Hazard and Risk Due to Induced Earthquakes at a Shale Gas Site. *Bulletin of the Seismological Society of America*, 111(2):875–897, Jan. 2021. doi: 10.1785/0120200234.

Esposito, S. and Iervolino, I. Spatial Correlation of Spectral Acceleration in European Data. *Bulletin of the Seismological Society of America*, 102(6):2781–2788, Dec. 2012. doi: 10.1785/0120120068.

Evensen, D., Varley, A., Whitmarsh, L., Devine-Wright, P., Dickie, J., Bartie, P., Napier, H., Mosca, I., Foad, C., and Ryder, S. Effect of linguistic framing and information provision on attitudes towards induced seismicity and seismicity regulation. *Scientific Reports*, 12(1), July 2022. doi: 10.1038/s41598-022-15448-4.

Foulger, G. R., Wilson, M. P., Gluyas, J. G., Julian, B. R., and Davies, R. J. Global review of human-induced earthquakes. *Earth-Science Reviews*, 178:438–514, Mar. 2018. doi: 10.1016/j.earscirev.2017.07.008.

Green, C., Styles, P., and Baptie, B. Preese Hall Shale Gas Fracturing Review and Recommendations for Induced Seismic Mitigation, Induced Seismicity. Mitigation report„ Department of Energy and Climate Change, London, 2012.

Heath, D. C., Wald, D. J., Worden, C. B., Thompson, E. M., and Smoczyk, G. M. A global hybrid Vs30 map with a topographic slope–based default and regional map insets. *Earthquake Spectra*, 36(3):1570–1584, June 2020. doi: 10.1177/8755293020911137.

Hicks, S. P., Verdon, J., Baptie, B., Luckett, R., Mildon, Z. K., and Gernon, T. A shallow earthquake swarm close to hydrocarbon activities: Discriminating between natural and induced causes for the 2018–2019 Surrey, United Kingdom, earthquake sequence. *Seismological Research Letters*, 90(6):2095–2110, Aug. 2019. doi: 10.1785/0220190125.

Hicks, S. P., Goes, S., Whittaker, A. C., and Stafford, P. J. Multivariate Statistical Appraisal of Regional Susceptibility to Induced Seismicity: Application to the Permian Basin, SW United States. *Journal of Geophysical Research: Solid Earth*, 126(12), Dec. 2021. doi: 10.1029/2021jb022768.

Jaiswal, K. and Wald, D. An Empirical Model for Global Earthquake Fatality Estimation. *Earthquake Spectra*, 26(4):1017–1037, Nov. 2010. doi: 10.1193/1.3480331.

Jaiswal, K., Wald, D., and Hearne, M. Estimating casualties for large earthquakes worldwide using an empirical approach. U.s geological survey open-file report, of 2009-1136„ 2009.

Kettlety, T., Verdon, J. P., Butcher, A., Hampson, M., and Craddock, L. High-resolution imaging of the ML 2.9 August 2019 earthquake in Lancashire, United Kingdom, induced by hydraulic fracturing during Preston New Road PNR-2 operations. *Seismological Research Letters*, 92(1):151–169, Oct. 2020. doi: 10.1785/0220200187.

Korswagen, P., Longo, M., Meulman, E., Licciardello, L., and Sousamli, M. *Damage Sensitivity of Groningen Masonry – Experimental and Computational Studies (Part 2*. NAM Report by Delft University of Technology, 2019.

Lei, X., Wang, Z., and Su, J. The December 2018 ML 5.7 and January 2019 ML 5.3 earthquakes in South Sichuan basin induced by shale gas hydraulic fracturing. *Seismological Research Letters*, 90(3):1099–1110, Apr. 2019. doi: 10.1785/0220190029.

Luckett, R., Ottemöller, L., Butcher, A., and Baptie, B. Extending local magnitude ML to short distances. *Geophysical Journal International*, 216(2):1145–1156, Nov. 2018. doi: 10.1093/gji/ggy484.

Majer, E., Nelson, J., Robertson-Tait, A., Savy, J., and Wong, I. Protocol for Addressing Induced Seismicity Associated with Enhanced Geothermal Systems. Technical report, Jan. 2012. doi: 10.2172/1219482.

Marzocchi, W., Iervolino, I., Giorgio, M., and Falcone, G. When Is the Probability of a Large Earthquake Too Small? *Seismological Research Letters*, 86(6):1674–1678, Sept. 2015. doi: 10.1785/0220150129.

Mignan, A., Broccardo, M., Wiemer, S., and Giardini, D. Induced seismicity closed-form traffic light system for actuarial decision-making during deep fluid injections. *Scientific Reports*, 7(1), Oct. 2017. doi: 10.1038/s41598-017-13585-9.

Monaghan, A. The Carboniferous shales of the Midland Valley of Scotland: geology and resource estimation. *British Geological Survey for Department of Energy and Climate Change*, page 105,

2014.

Mosca, I., Sargeant, S., Baptie, B., Musson, R. M. W., and Pharaoh, T. C. The 2020 national seismic hazard model for the United Kingdom. *Bulletin of Earthquake Engineering*, 20(2):633–675, Jan. 2022. doi: 10.1007/s10518-021-01281-z.

Musson, R. British earthquakes. *Proceedings of the Geologists' Association*, 118(4):305–337, Jan. 2007. doi: 10.1016/s0016-7878(07)80001-0.

Musson, R. M. W. A critical history of British earthquakes. *Annals of Geophysics*, 47(2-3), Dec. 2004. doi: 10.4401/ag-3325.

Nievas, C. I., Bommer, J. J., Crowley, H., and van Elk, J. Global occurrence and impact of small-to-medium magnitude earthquakes: a statistical analysis. *Bulletin of Earthquake Engineering*, 18(1):1–35, Sept. 2019. doi: 10.1007/s10518-019-00718-w.

Oil and Gas Authority. Consolidated Onshore Guidance, Version 2.2, North Sea Transition Authority Report, 2018. https://www.nstauthority.co.uk/media/4908/consolidated-onshore-guidance-compendium_vfinal12062018.pdf.

Pater, C. and Baisch, S. Geomechanical study of Bowland Shale seismicity. page 71, 2011.

Pawley, S., Schultz, R., Playter, T., Corlett, H., Shipman, T., Lyster, S., and Hauck, T. The Geological Susceptibility of Induced Earthquakes in the Duvernay Play. *Geophysical Research Letters*, 45 (4):1786–1793, Feb. 2018. doi: 10.1002/2017gl076100.

Redmayne, D. W. Mining induced seismicity in UK coalfields identified on the BGS National Seismograph Network. *Geological Society, London, Engineering Geology Special Publications*, 5(1): 405–413, Jan. 1988. doi: 10.1144/gsl.eng.1988.005.01.45.

Redmayne, D. W., Richards, J. A., and Wild, P. W. Mining-induced earthquakes monitored during pit closure in the Midlothian Coalfield. *Quarterly Journal of Engineering Geology*, 31(1): 21–36, Feb. 1998. doi: 10.1144/gsl.qjeg.1998.031.p1.03.

Rose, A., McKee, J., Urban, M., Bright, E., and Sims, K. LandScan 2018 High-Resolution Global Population Data Set (No. In *LandScan 2018 High-Resolution Global Population Da; 005854MLTPL00). Oak Ridge National Laboratory (ORNL*. Oak Ridge, TN, 2019. United States).

Roy, C., Nowacki, A., Zhang, X., Curtis, A., and Baptie, B. Accounting for Natural Uncertainty Within Monitoring Systems for Induced Seismicity Based on Earthquake Magnitudes. *Frontiers in Earth Science*, 9, May 2021. doi: 10.3389/feart.2021.634688.

Schultz, R., Atkinson, G., Eaton, D. W., Gu, Y. J., and Kao, H. Hydraulic fracturing volume is associated with induced earthquake productivity in the Duvernay play. *Science*, 359(6373): 304–308, Jan. 2018. doi: 10.1126/science.aao0159.

Schultz, R., Beroza, G., Ellsworth, W., and Baker, J. Risk-informed recommendations for managing hydraulic fracturing induced seismicity via traffic light protocols. *Bulletin of the Seismological Society of America*, 110(5):2411–2422, Apr. 2020a. doi: 10.1785/0120200016.

Schultz, R., Skoumal, R. J., Brudzinski, M. R., Eaton, D., Baptie, B., and Ellsworth, W. Hydraulic Fracturing-Induced Seismicity. *Reviews of Geophysics*, 58(3), July 2020b. doi: 10.1029/2019rg000695.

Schultz, R., Beroza, G. C., and Ellsworth, W. L. A risk-based approach for managing hydraulic fracturing-induced seismicity. *Science*, 372(6541):504–507, Apr. 2021a. doi: 10.1126/science.abg5451.

Schultz, R., Beroza, G. C., and Ellsworth, W. L. A Strategy for Choosing Red-Light Thresholds to Manage Hydraulic Fracturing Induced Seismicity in North America. *Journal of Geophysical Research: Solid Earth*, 126(12), Dec. 2021b. doi: 10.1029/2021jb022340.

Schultz, R., Quitoriano, V., Wald, D. J., and Beroza, G. C. Quantifying nuisance ground motion thresholds for induced earthquakes. *Earthquake Spectra*, 37(2):789–802, Jan. 2021c. doi: 10.1177/8755293020988025.

Schultz, R., Ellsworth, W. L., and Beroza, G. C. Statistical bounds on how induced seismicity stops. *Scientific Reports*, 12(1), Jan. 2022a. doi: 10.1038/s41598-022-05216-9.

Schultz, R., Muntendam-Bos, A., Zhou, W., Beroza, G. C., and Ellsworth, W. L. Induced seismicity red-light thresholds for enhanced geothermal prospects in the Netherlands. *Geothermics*, 106:102580, Dec. 2022b. doi: 10.1016/j.geothermics.2022.102580.

Smith, D. C. and Richards, J. M. Social License to Operate: Hydraulic Fracturing-Related Challenges Facing the Oil & Gas Industry. *SSRN Electronic Journal*, 2015. doi: 10.2139/ssrn.2591988.

Smith, N., Turner, P., and Williams, G. UK data and analysis for shale gas prospectivity. *Geological Society, London, Petroleum Geology Conference Series*, 7(1):1087–1098, Jan. 2010. doi: 10.1144/0071087.

SodM, Staatstoezicht op de Mijnen. Risico analyse aardgasbevingen Groningen (Risk assessment gas-earthquakes Groningen, in Dutch), 2014.

Thomas, M., Partridge, T., Harthorn, B. H., and Pidgeon, N. Deliberating the perceived risks, benefits, and societal implications of shale gas and oil extraction by hydraulic fracturing in the US and UK. *Nature Energy*, 2(5), Apr. 2017. doi: 10.1038/nenergy.2017.54.

UK Public General Acts. UK Infrastructure Act 2015, 2015. https://www.legislation.gov.uk/ukpga/2015/7/part/6/crossheading/other-provision-about-onshore-petroleum/enacted.

U.N.-P.D. United Nations Department of Economic and Social Affairs Population Division, 2022. https://population.un.org/wpp/. World Population Prospects 2022, Online Edition.

van der Voort, N. and Vanclay, F. Social impacts of earthquakes caused by gas extraction in the Province of Groningen, The Netherlands. *Environmental Impact Assessment Review*, 50: 1–15, Jan. 2015. doi: 10.1016/j.eiar.2014.08.008.

Verdon, J. P. and Bommer, J. J. Green, yellow, red, or out of the blue? An assessment of Traffic Light Schemes to mitigate the impact of hydraulic fracturing-induced seismicity. *Journal of Seismology*, 25(1):301–326, Oct. 2020. doi: 10.1007/s10950-020-09966-9.

Verdon, J. P. and Rodríguez-Pradilla, G. Assessing the variability in hydraulic fracturing-induced seismicity occurrence between North American shale plays. *Tectonophysics*, 859:229898, July 2023. doi: 10.1016/j.tecto.2023.229898.

Villani, M., Polidoro, B., McCully, R., Ader, T., Edwards, B., Rietbrock, A., Lubkowski, Z., Courtney, T. J., and Walsh, M. A Selection of GMPEs for the United Kingdom Based on Instrumental and Macroseismic Datasets. *Bulletin of the Seismological Society of America*, 109(4):1378–1400, July 2019. doi: 10.1785/0120180268.

Wald, D. J., Quitoriano, V., Worden, C. B., Hopper, M., and Dewey, J. W. USGS "Did You Feel It?" internet-based macroseismic intensity maps. *Annals of Geophysics*, 54(6), Jan. 2012. doi: 10.4401/ag-5354.

Westlake, S., John, C. H. D., and Cox, E. Perception spillover from fracking onto public perceptions of novel energy technologies. *Nature Energy*, 8(2):149–158, Jan. 2023. doi: 10.1038/s41560-022-01178-4.

Williams, L., Macnaghten, P., Davies, R., and Curtis, S. Framing 'fracking': Exploring public perceptions of hydraulic fracturing

in the United Kingdom. *Public Understanding of Science*, 26(1): 89–104, Aug. 2016. doi: 10.1177/0963662515595159.

Wilson, M. P., Davies, R. J., Foulger, G. R., Julian, B. R., Styles, P., Gluyas, J. G., and Almond, S. Anthropogenic earthquakes in the UK: A national baseline prior to shale exploitation. *Marine and Petroleum Geology*, 68:1–17, Dec. 2015. doi: 10.1016/j.marpetgeo.2015.08.023.